

Evidence for Deep Magma Injection Beneath Lake Tahoe, Nevada-California

Kenneth D. Smith,^{1*} David von Seggern,¹ Geoffrey Blewitt,^{1,2}
Leiph Preston,¹ John G. Anderson,¹ Brian P. Wernicke,³
James L. Davis⁴

A deep earthquake swarm in late 2003 at Lake Tahoe, California (Richter magnitude < 2.2; depth of 29 to 33 kilometers), was coeval with a transient displacement of 6 millimeters horizontally outward from the swarm and 8 millimeters upward measured at global positioning system station Slide Mountain (SLID) 18 kilometers to the northeast. During the first 23 days of the swarm, hypocentral depths migrated at a rate of 2.4 millimeters per second up-dip along a 40-square-kilometer structure striking north 30° west and dipping 50° to the northeast. SLID's transient velocity of 20 millimeters per year implies a lower bound of 200 nanostrains per year (parts per billion per year) on local strain rates, an order of magnitude greater than the 1996 to 2003 regional rate. The geodetic displacement is too large to be explained by the elastic strain from the cumulative seismic moment of the sequence, suggesting an aseismic forcing mechanism. Aspects of the swarm and SLID displacements are consistent with lower-crustal magma injection under Lake Tahoe.

The 12 to 14 mm/year of northwest-directed motion of the Sierra Nevada mountain range in eastern California and western Nevada relative to stable North America represents about 20 to 25% of the Pacific–North America plate motion budget (1, 2). At the latitude of Lake Tahoe, California–Nevada, much of this shear and extension is concentrated in the westernmost Great Basin, characterized at the surface by strike-slip and normal faulting. The eastern boundary of the Sierra Nevada is a geologically young transition marked by north-striking, east-dipping normal fault systems that account for Great Basin extension, the westward evolution of the Sierra Nevada–to–Great Basin transition, and the consequent eastward collapse of the competent Sierra Nevada block. Paleozoic and Mesozoic roof pendants and Cretaceous granites in the region are overlain by volcanic rocks from the Miocene to about 3 million years ago (Ma) and by a distinct younger period, from 1 to 2 Ma, of localized rhyolitic and basaltic magmatism (3).

The shallow crust in the California–Nevada border region near Lake Tahoe includes north-south–striking normal faults and north-east- and northwest-striking strike-slip faults operating within east-west–oriented regional extension (σ_3). This is a consequence of the near equivalence of the maximum and inter-

mediate (σ_1 and σ_2) compressive stresses (4, 5). The base of the seismogenic zone in the region varies locally from about 15 to 18 km (6). In the Lake Tahoe area, no crustal earthquakes deeper than 20 km can be identified from more than 25 years of monitoring.

In a map view, the deep crustal sequence of earthquakes observed in 2003 straddles the northwest shore of Lake Tahoe and defines a planar structure of 8 by 5 km striking N30°W and dipping 50°NE between depths of 29 and 33 km (Fig. 1 and fig. S1). A total of 1611 earthquakes were located in the swarm [sum of the moment magnitude (M_w) of all events is 3.1], and the 1179 best-located events are shown [supporting online material (SOM) text]. The swarm began with a 0.0-magnitude event on 12 August 2003 and continued through 19 February 2004. Fifteen earthquakes on 31 December 2003 and 1 January 2004 marked the last days with more than one located event, and the last events of the swarm (as of 26 July 2004) occurred on 5, 8, 12, and 20 January and 19 February 2004. Daily activity rates are peaked at times when the earthquake depths are shallower (Fig. 2). The final temporal concentration of seismicity began on 22 November 2003 and peaked with 88 earthquakes on 27 November 2003 (Fig. 2A). Seismograms of the deep events resemble shallow tectonic earthquakes near Lake Tahoe that have impulsive *P*-wave arrivals and high-frequency waveforms. However, no long-period (LP) earthquakes, generally thought to result from magma movement in the crust, have been identified.

Hypocentral depths progressed from about 33 to 29 km (relative to the elevation of Lake Tahoe) by 3 September 2003 at a rate

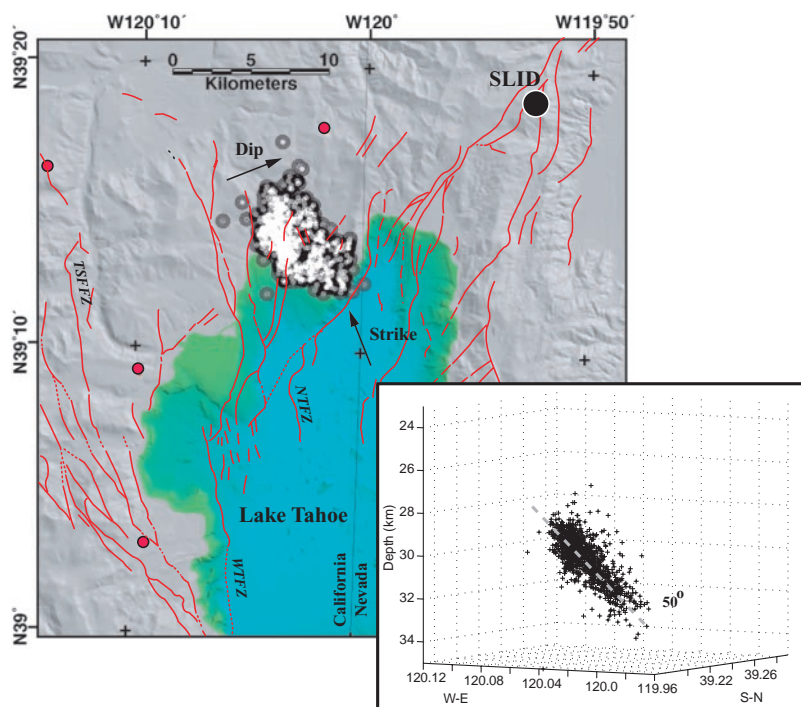


Fig. 1. Deep earthquake activity (>20 km) in the Lake Tahoe, California area, 2003 to 2004, and location of GPS station SLID and faults with Holocene displacement (8). Red circles mark seismic stations. Major east-dipping normal faults: TSFFZ, Tahoe-Sierra frontal fault zone; WTFZ, West Tahoe fault zone; NTFZ, North Tahoe fault zone. Inset shows cross-sectional view along strike, N30°W, of inferred structure at depth.

¹Nevada Seismological Laboratory, ²Nevada Bureau of Mines and Geology, University of Nevada, Reno, NV 89557, USA. ³Division of Geological and Planetary Sciences, California Institute of Technology, Pasadena, CA 92215, USA. ⁴Harvard-Smithsonian Center for Astrophysics, Cambridge, MA 02138, USA.

*To whom correspondence should be addressed. E-mail: ken@seismo.unr.edu

REPORTS

(\pm SD) of 2.4 ± 0.6 mm/s (8.5 m/hour) up-dip along the imaged planar structure (Fig. 2B). The temporal and spatial depth distribution implies a source propagating up-dip that had reached its shallowest extent by 3 September 2003, 23 days into the sequence (Fig. 2B). This is consistent with the leading edge of a volcanic dike intrusion where earthquakes are triggered by high strain rates and localized stresses at the injection front (7, 8).

An increase in the upper crustal seismicity (depth of <18 km) began about 2 months after the initiation of the deep-crustal sequence (fig. S2) and continued through June 2004. The largest of the shallow events occurred on 3 June 2004: an M_w 4.2 earthquake at a depth of 8.5 km, about 10 km north-northeast of the epicentral region of the deep swarm. Including the 2004 event, the Nevada Seismological Laboratory catalog lists eight earthquakes with Richter magnitudes ($M_L \geq 4.2$ since 1950 within 30 km of the center of North Lake Tahoe. The mean rate is one event this size or larger every 6 to 7 years. The Coulomb failure function on shallow faults was probably altered, consistent with the increase in shallow seismicity.

Magnitudes for the Lake Tahoe deep swarm range from $M_L -0.2$ to 2.2 with a b value of 2.0 (SOM text) (b is the slope in the regression equation $\log_{10} N = a - bM$, where N is the number of events at magnitude M). When b values are much greater than 1.0, they are anomalous for upper-crustal tectonic earthquakes but typical of volcanic regions (9, 10). In the Long Valley volcanic area, Wiemer *et al.* (11) found b values as high as 1.8 for upper-crustal sequences associated with upper-crustal volcanic processes.

Double-couple focal mechanism solutions have been determined for the 24 largest events ($M_L > 1.5$) with a combination of P -wave first-motion polarities and P - and S -wave amplitudes (fig. S3 and SOM text). With one exception, all have a reverse-faulting component. Most solutions are consistent with zones of weakness moved to failure by a maximum compressive stress oriented 225° and plunging 30° SW (fig. S4). The maximum compressive stress (σ_1) is aligned approximately normal to the imaged structure, consistent with tensile failure along the northeast-dipping structure (7). Among the reverse-faulting events, the T axes strike northeast, but over a wide range (fig. S4). This is in contrast to regional east-west-oriented extension observed in upper-crustal focal mechanisms that are consistent with normal fault orientations near Lake Tahoe (4, 12). A possible explanation is that the stress field is locally perturbed by processes within the volume of the swarm.

A continuously recording geodetic global positioning system (GPS) station on the summit of

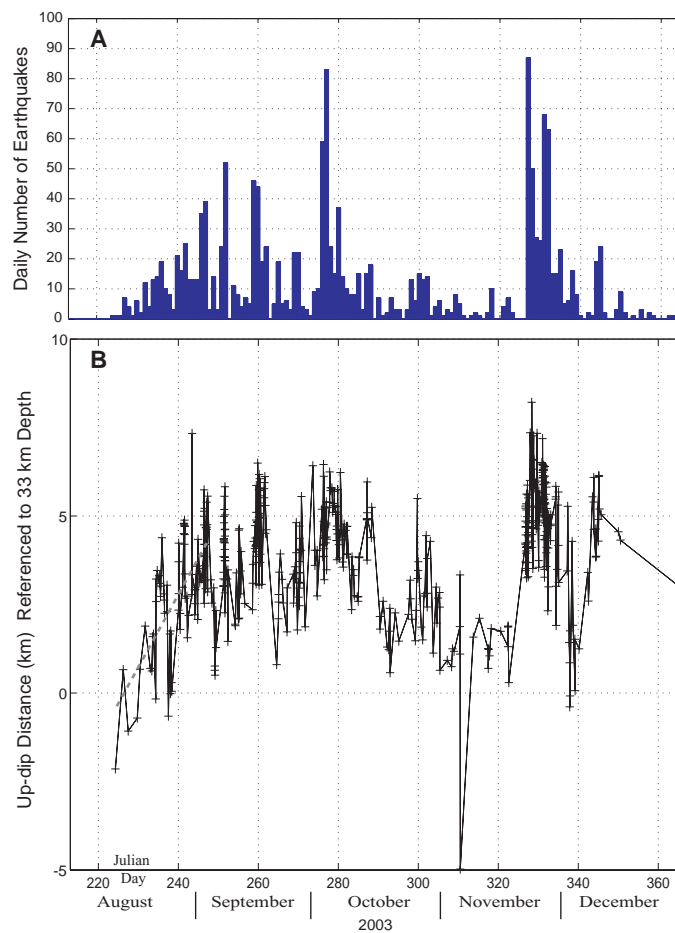


Fig. 2. (A) Daily number of earthquakes for all located deep events. (B) Temporal progression of earthquake depths relative to 33-km depth along up-dip distance of lower-crustal inferred structure. The dashed line is a rate of 2.4 mm/s from 12 August through 3 September 2003.

Slide Mountain (SLID, Fig. 1) is located horizontally 18 km away at $N60^\circ E$ from the center of the swarm region and 31 km obliquely from the center of the northeast-dipping imaged planar structure at depth, nearly perpendicular to the plane. SLID is part of the 53-station Basin and Range Geodetic Network (BARGEN), which has operated continuously since 1996 to investigate tectonic deformation in the Basin and Range Province (2, 13). The same instrument design (including receiver, antenna, radome, and deep-anchored braced monument) has been implemented at all BARGEN stations in the region of SLID without changes since December 1999. Therefore, our geodetic analysis started on 1 January 2000, including data through 28 June 2004.

GPS data from SLID were processed with data from the five nearest BARGEN stations (UPSA, GARL, SHIN, GABB, and TUNG; 99 to 184 km from SLID in Fig. 4) in 24-hour batches with the GIPSY OASIS II software to produce six time series of three-dimensional (3D) precise point positions (longitude, latitude, and ellipsoidal height) relative to ITRF2000 (14–16). Each station's coordinate time series was detrended and then regionally filtered (17) by subtracting the mean time series from the five neighboring stations. An-

nual periodic signals were then removed (18), and finally 7-day averages were formed (Fig. 3). The estimated annual signals have a mean amplitude of 0.3 mm in horizontal components and 0.9 mm in height. The weekly time series have a 1-SD scatter of 0.5 mm in horizontal components and 2.1 mm in height, before July 2003. The scales of the formal error bars were adjusted to be consistent with this scatter (SOM text).

In contrast to neighboring BARGEN stations, all three SLID coordinates underwent episodic displacement starting in July 2003 and lasting 6 months, coeval with the deep crustal seismicity. The difference in mean coordinates between the periods from January to June 2004 and from January to June 2003 were taken as displacement estimates, yielding 3.1 ± 0.2 mm northward, 4.9 ± 0.3 mm eastward, and 7.9 ± 1.0 mm upward (error of 1 SD). The SLID 2D horizontal displacement of 5.8 mm is oriented $N58^\circ E$, approximately in the direction of SLID relative to the source region, with the 3D vector displacement of 9.8 mm aligned approximately normal to the planar structure at depth (Fig. 1). In contrast, for the five neighboring stations the root mean square of estimated displacements is 0.4 mm for horizontal components, 0.7 mm for height, and 0.9 mm in total distance. These numbers provide a realistic estimate of the total

Fig. 3. GPS coordinate time series for SLID and neighboring stations in each of three component directions. Data displayed are 7-day averages with scaled formal error bars of 1 SD. Coordinate axes for SLID are extended to accommodate the signal, but the scale is the same for all stations for a given component. The scale of the height component is a factor of 3 greater than for the horizontal components to visually normalize the higher level of noise in height.

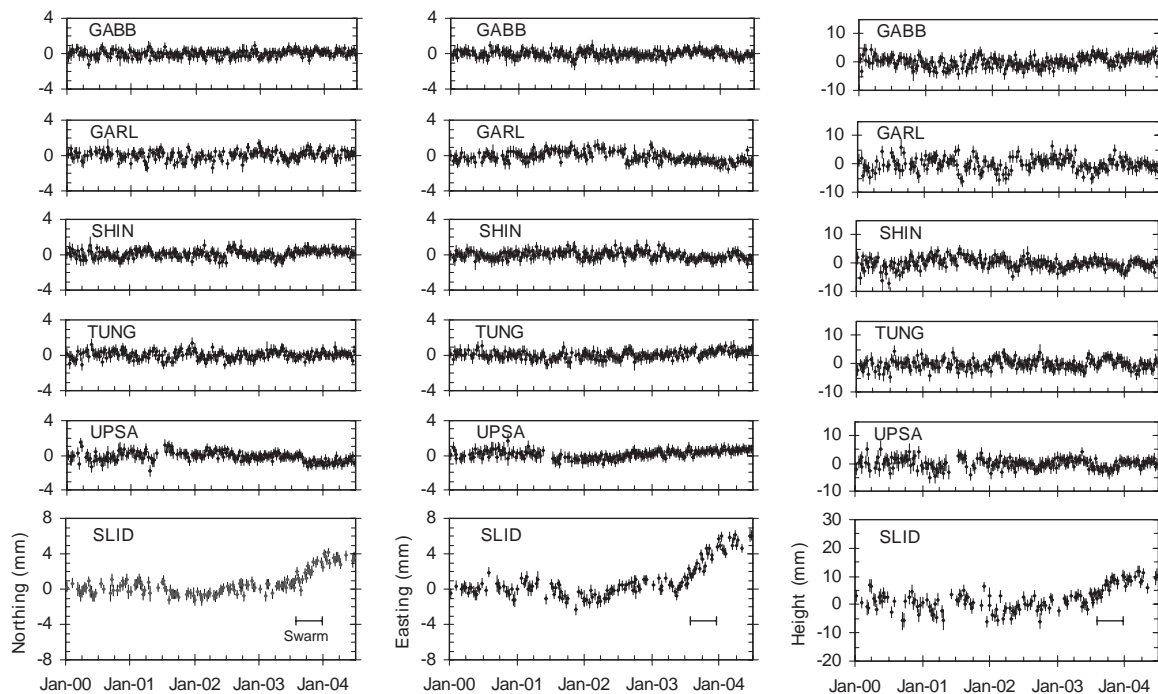
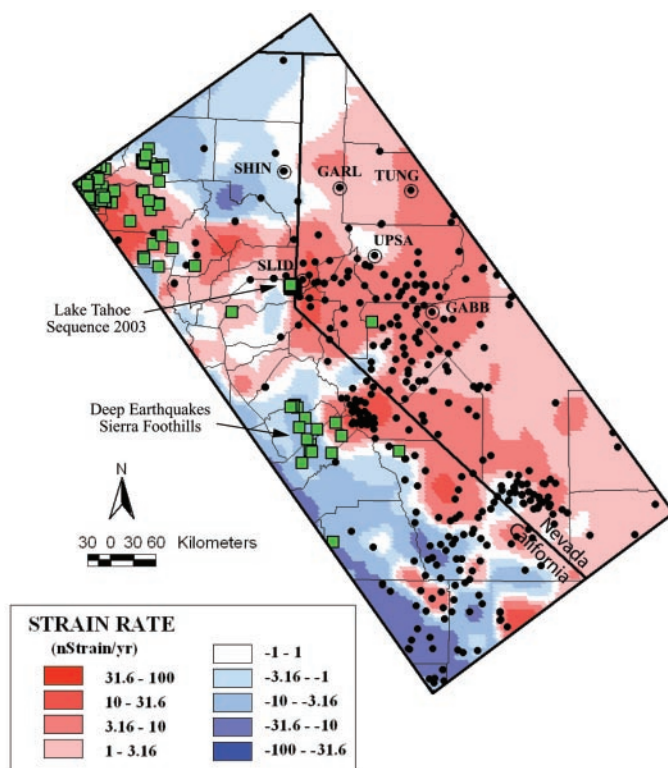


Fig. 4. Dilatational strain map determined from GPS stations in the Sierra Nevada region. Black circles are stations used in calculating dilatational strain in nanostrains per year (nstrain/yr) and circles within circles are BARGEN array stations. Best-located events from the Advanced National Seismic System (ANSS) earthquake catalog between depths of 20 and 50 km (green squares) are included.



error in SLID's displacement and are consistent to within 2 SD of the formal errors.

These results yield a transient change in velocity of SLID between July 2003 and January 2004 of 20 ± 2 mm/year (12 ± 1 mm/year horizontally). This in turn implies a lower bound on transient strain rates of ~ 200 nanostrains per year (120 nanostrains per year horizontally) in the region between

SLID and neighboring stations. These rates are several times higher than (and in addition to) the 1996 to 2003 regional strain rate of 30 to 40 nanostrains per year reported from BARGEN observations before the transient event (2), and an order of magnitude greater than the estimated errors.

The extent of fault rupture is typically estimated from aftershock distributions. The

area of the planar structure at depth (40 km^2), assuming a stress drop of 10 MPa (reasonable for upper-crustal earthquakes), would cause a seismic moment equivalent to an M_w of 6.0 and displacement of ~ 1 m at the source. Reverse faulting on the imaged structure at depth (hanging wall up and to the southwest) would result in horizontal displacements at SLID up and to the southwest, so the horizontal component would be in the opposite direction of the observations. Normal faulting, on the other hand, although characteristic of the Lake Tahoe region, would result in a loss of elevation at SLID. However, a dilatational mechanism can fit the geodetic data. Applying Okada's (19) model for a tensile crack at 30-km depth in the source region, a potency equivalent to a volume of $3.7 \times 10^7 \text{ m}^3$, or a volumetric moment equivalent to M_w 6.1, fits the SLID observations (SOM text). Because only one GPS station is available, the source of the displacements at SLID cannot be uniquely determined. Mechanisms such as the introduction of fluids in the volume between the deep swarm and SLID or volumetric expansion of a potential source of magma below the deep-crustal swarm could be developed to fit SLID motions.

The temporal correlation of SLID motions and deep seismicity strongly suggests that the source of SLID displacements is spatially correlated with the earthquake swarm. SLID motions are not consistent with a shear dislocation but with dilatational or tensile failure, along the deep structure. Also, the progression of earthquake depths and stress field implied from earthquake focal mechanisms is consistent with other observations of dike intrusion (8). In addition, the high b value of

the Lake Tahoe sequence is most likely in response to rock failure due to a high strain rate, typical of dike injection (7). The injection front of a propagating dike is reflected by the temporal progression of earthquake depths, whereas the high-frequency character of the events requires brittle failure of rock at the crack tip. Also, tensile failure along east-dipping structures would be consistent with east-west extension along the Great Basin Sierra Nevada transition near Lake Tahoe. High dilatational strain rates are inferred from GPS data in the Lake Tahoe region (Fig. 4). SLID deformation and the character of the earthquake swarm are consistent with magma injection. The volumetric source required to fit SLID observations would correspond to a ~1-m-thick dike over the area of the imaged structure at depth. Dipping eastward at 50°, the lower-crustal structure would project to the surface west of the Sierra Nevada Great Basin frontal fault system west of Lake Tahoe. However, if a Sierra Nevada/Great Basin–bounding structure, or structural zone, shallows eastward into the lower crust, the event may have taken place near or within this structural boundary.

Periodic aseismic transient deformation in the Cascadia subduction zone is associated with deep-crustal LP earthquakes (25 to 45 km in depth) with tremor-like seismic signatures (20, 21). Outside of subduction regions, however, deep brittle–failure earthquakes are uncommon because of the predominance of a brittle–ductile transition in the mid-crust and increased temperature with depth. Brittle failure at these depths requires localized high strain rates that can result from magma injection. Deep earthquakes observed in the western Sierra Nevada foothills (22) may be in response to the same mechanism (Fig. 4). We suggest that this magmatic phenomenon should not be viewed as a likely precursor to volcanism, but rather as part of the tectonic cycle of lower-crustal evolution, perhaps providing a mechanism to sustain crustal thickness and crustal strength in zones of extension.

References and Notes

1. T. Dixon, M. Miller, F. Farina, H. Wang, D. Johnson, *Tectonics* **19**, 1 (2000).
2. R. Bennett, B. Wernicke, N. Niemi, A. Friedrich, J. Davis, *Tectonics* **22**, 1008.10.1029/2001TC001355 (2003).
3. C. Henry, J. Faulds, abstract presented at the EarthScope/NSF Great Basin Symposium, Lake Tahoe, California, 21 to 23 June 2004.
4. R. Schweickert, M. Lahren, K. Smith, J. Howle, *Tectonophysics*, in press.
5. S. Wesnousky, C. Jones, *Geology* **22**, 1031 (1994).
6. Nevada Seismological Laboratory Historical Earthquake Catalog, accessible and searchable at www.seismo.unr.edu/Catalog/catalog-search.html.
7. A. Rubin, D. Pollard, *Geology* **16**, 413 (1988).
8. M. Ukawa, H. Tsukahara, *Tectonophysics* **253**, 285 (1996).
9. S. R. McNutt, *International Handbook of Earthquake and Engineering Seismology, Part A* (Academic Press, Amsterdam, Netherlands, 2002), pp. 383–406.

10. V. Zobin, *Introduction to Volcanic Seismology* (Elsevier, Amsterdam, Netherlands, 2003).
11. S. Wiemer, S. McNutt, M. Wyss, *Geophys. J. Int.* **134**, 409 (1998).
12. G. Ichinose, J. Anderson, K. Smith, Y. Zeng, *Bull. Seism. Soc. Am.* **93**, 61 (2003).
13. B. Wernicke, A. Friedrich, N. Niemi, R. Bennett, J. L. Davis, *GSA Today* **10**, 1 (2000).
14. J. Zumberge, M. Heflin, D. Jefferson, M. Watkins, F. Webb, *J. Geophys. Res.* **102**, 5005 (1997).
15. G. Blewitt, *J. Geophys. Res.* **94**, 10187 (1989).
16. Z. Altamimi et al., *Eos* **82**, 273 (2001).
17. S. Wdowinski, Y. Bock, J. Zhang, P. Fang, J. Genrich, *J. Geophys. Res.* **102**, 18057 (1997).
18. G. Blewitt, D. Lavallée, *J. Geophys. Res.* **107**, 2145, 10.1029/2001JB000570 (2002).
19. Y. Okada, *Bull. Seism. Soc. Am.* **75**, 1135 (1985).
20. H. Dragert, K. Wang, T. James, *Science* **292**, 1525 (2001).
21. G. Rogers, H. Dragert, *Science* **300**, 1942 (2003).
22. I. Wong, W. Savage, *Bull. Seism. Soc. Am.* **73**, 797 (1983).
23. The University of Nevada, Reno seismic network in northern Nevada is operated under the U.S. Geological Survey National Earthquake Hazards Reduction Program with support from the State of Nevada. The

GPS data analysis was funded by the Department of Energy, Yucca Mountain Project. The BARGEN GPS network is funded by NSF and the Department of Energy, with operational support from UNAVCO, Inc. The GIPSY OASIS II software and global GPS data products were provided by the Jet Propulsion Laboratory. We thank G. Oppliger for a review of the manuscript and M. Coolbaugh for generating the regional strain map figure. Several stations in the Nevada K-12 seismic network, Storey County High School, Carson City High School, and Douglas County High School contributed phase arrival data for constraining earthquake locations in the lower-crustal swarm. We thank three anonymous reviewers for their time and effort in reviewing the manuscript.

Supporting Online Material

www.sciencemag.org/cgi/content/full/1101304/DC1
SOM Text
Figs. S1 to S4
References

9 June 2004; accepted 28 July 2004
Published online 5 August 2004;
10.1126/science.1101304
Include this information when citing this paper.

Powering Fuel Cells with CO via Aqueous Polyoxometalates and Gold Catalysts

Won Bae Kim, T. Voitl, G. J. Rodriguez-Rivera, J. A. Dumesic*

Electricity was produced by catalytic oxidation of carbon monoxide (CO) by using gold catalysts at room temperature. The observed rates are faster than conventional processes operating at 500 kelvin or higher for the conversion of CO with water to produce hydrogen and carbon dioxide through the water-gas shift (WGS). By eliminating the WGS reaction, we remove the need to transport and vaporize liquid water in the production of energy for portable applications. This process can use CO-containing gas streams from the catalytic reforming of hydrocarbons to produce an aqueous solution of reduced polyoxometalate compounds that can be used to generate power. The reduced polyoxometalate can be reoxidized in fuel cells that contain simple carbon anodes.

The production of H₂ for fuel cells typically involves the initial formation of a mixture of H₂, CO, and CO₂ from hydrocarbons or oxygenated hydrocarbons (1–5), followed by the water-gas shift (WGS) reaction (CO + H₂O → CO₂ + H₂) to achieve the high conversions of CO to CO₂ (6–9) necessary for proton-exchange membrane (PEM) fuel cells, in view of the strong poisoning effects of CO on Pt-based anodes (10). The WGS reaction represents a major bottleneck in the production of H₂ because this exothermic reaction is slow at the low temperatures (~500 K) required to achieve favorable equilibrium conversions. In addition, the WGS reaction imposes an important limitation for the production of H₂ for portable applications because large amounts of liquid water must

be transported and vaporized. Here, we demonstrate a process that bypasses the WGS reaction during the production of fuel-cell-grade H₂ by using the CO directly as an additional source of energy from H₂ streams. This process is especially promising for the production of electrical energy from renewable biomass-derived oxygenated hydrocarbons because these reactants have C:O stoichiometric ratios equal to 1:1, and they therefore generate H₂ and CO in nearly equal amounts during catalytic decomposition.

Our process for oxidation and use of CO involves the reaction of CO and liquid water with a reducible polyoxometalate (POM) compound, such as H₃PMO₁₂O₄₀, that serves as a strong oxidizing agent for CO and as an energy-storage agent for electrons and protons, over gold nanotubes or nanoparticles, and it takes advantage of the high catalytic activities of gold nanoparticles for CO oxidation (11–13), especially in the presence of liquid water (14, 15). This catalytic process

Department of Chemical and Biological Engineering, University of Wisconsin, Madison, WI 53706, USA.

*To whom correspondence should be addressed. E-mail: dumesic@engr.wisc.edu